15

Recovery of EUV optical constants of thin films using laboratory reflectometry data

© N.V. Zagainov, S.A. Garakhin, S.S. Morozov, V.N. Polkovnikov, N.I. Chkhalo

Institute for Physics of Microstructures, Russian Academy of Sciences
603087 Nizhny Novgorod
e-mail: kolazagaunow41@gmail.com

Received May 29, 2025
Revised May 29, 2025
Accepted May 29, 2025

The study has investigated whether laboratory reflectometry methods may be used for measuring optical constants of materials in extreme ultraviolet (EUV) range. Analysis has been performed on tantalum compounds used as absorbers for mask blanks. Experiment for reflection coefficient measurement depending on the wavelength and angle of incidence for lithographic mask absorber layers has been numerically simulated. The model considers real specifications of laboratory devices and measurement errors. Numerical experiment has shown that laboratory reflectometry was applicable to identification of parameters of thin films on substrates, and it has been proved experimentally that the method was suitable for real applications. Such structural parameters as densities, roughnesses and thicknesses can be recovered with high accuracy. Deviations of all experimental measurements from simulated values are less than 1 %, the experiment has shown good accuracy for optical constant recovery.

Keywords: thin films, reflectometry, optical constants, tantalum, absorption, diffractometer, reflectometer, reflection coefficient, X-ray radiation, X-ray lithography.

DOI: 10.61011/TP.2025.10.62085.120-25

Introduction

There is currently a rapid growth of extreme ultraviolet lithography technology [1–4]. Reflective masks are one of the lithographic process components. Since modern chips have a multilayer structure, up to 80 lithographic masks may be required to create one integrated circuit configuration. Most of them are still made using an ultraviolet lithography technique (operating wavelength of 193 nm). However, even now up to one third of masks for an integrated circuit are made for lithographic processes with an operating wavelength of 13.5 nm. These are so-called EUV (extreme ultraviolet) masks. Thus, quality control of such masks becomes increasingly important.

EUV mask-blanks are multilayer thin-film structures on a substrate [5]. This is actually an X-ray optics technology product. Mask layers are made by ion-beam sputtering that offers minimized amount of defects in a multilayer mirror structure [6]. Very high quality requirements are imposed to the layers.

Schematic diagram of a mask-blank is shown in Figure 1.

Each of the layers is described in detail below. The lowest layer, which is actually a component rather than a layer, is a substrate. It shall be made of a material with a low thermal coefficient of linear expansion (TCLE) and low RMS surface roughness. Fused silica and optical ceramic wafers with TCLE in the order of $10^{-8}\,K^{-1}$ are used as substrates in most cases.

The next bottom layer is reflective coating. This is a multilayer X-ray mirror designed to reflect the light transmitted through „windows“ in the top layers. The mirror shall have as high as possible reflection coefficient for the operating wavelength. Mirrors on the basis of Mo/Si pair with a period about 7 nm and a number of periods of 50 [7,8] are generally used for operation at 13.5 nm. Such mirrors with boron or carbon carbide barrier layers have a reflection coefficient up to 70 % at 13.5 nm. This value may be only achieved on supersmooth substrates with RMS surface roughness in the order of 0.2 nm. Hence, high requirements are imposed to substrate surface roughness. Moreover, it is known that Mo/Si mirrors have high temporal stability of reflective properties.

The X-ray mirror is followed by a protective layer. It is intended to protect the multilayer mirror against external impacts of both environment (sometimes aggressive) and plasma etching processes. A thin (about 2.5 nm) Ru film is often used as a protective layer.

A buffer layer is often deposited above the Ru film. Besides protecting the underlying layers against plasma

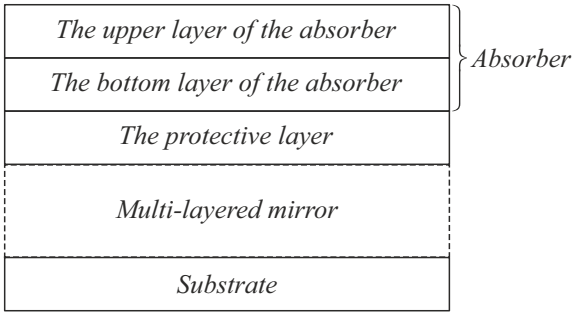

Figure 1. Schematic diagram of a mask-blank.

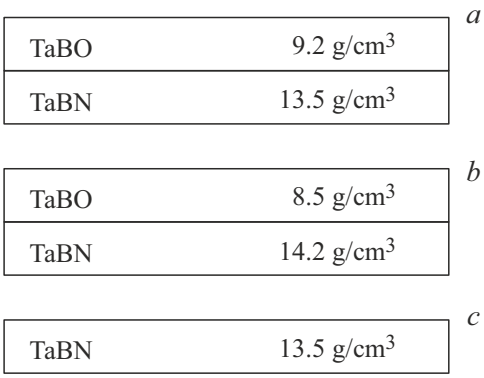

Figure 2. Possible mask-blank structures.

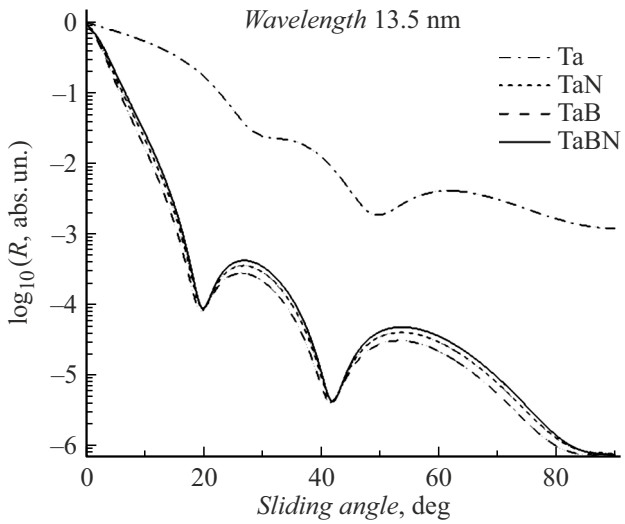

Figure 3. Angular dependences of reflection coefficients on the angle of incidence for tantalum-containing films.

etching processes, this layer prevents roughness inheritance by the top structure. For example, a 20 nm chromium nitride film may serve as a buffer layer.

The uppermost layer is an absorber layer. It is intended to absorb light that strikes the mask. Since the mask shall effectively absorb light (except for open layers in absorber and layers before the X-ray mirror), this layer consists of materials having high absorption coefficient at the operating wavelength. The main requirement for this structure, besides absorption properties, is its amorphous state. Amorphous structure is necessary for producing even mask edges (of open windows on the surface) after plasma etching. Plasma etching provides the desired pattern on the final product. In the areas where the absorber is removed, radiation reaches the multilayer X-ray mirror and is reflected from it. In places where the absorber is maintained, radiation is absorbed without reaching the reflective layer.

The absorber layer itself can generally consist of several layers. The point is that a multilayer (consisting of more than one layer) structure provides more effective radiation absorption. Thickness measurement provides the desired interference between rays reflected from different layers. This interference allows reduction of radiation reflected from the whole absorber. Absorber composition options in accordance with the data from [5] are shown in Figure 2.

As can be seen (Figure 2), mask-blank at 13.5 nm uses tantalum-containing materials as the absorber layer. Tantalum has a relatively high absorption in the spectral vicinity of 13.5 nm. For example, a 20 nm Ta film absorbs about 50 % of 13.5 nm radiation, and a 50 nm film already absorbs about 80 %; a 100 nm Ta film absorbs more than 95 % of radiation.

Calculations show that films containing tantalum compounds with other elements much more effectively suppress 13.5 nm radiation. Figure 3 shows angular dependences of reflection coefficients for 13.5 nm on different 20 nm tantalum-containing films (with tabular densities and zero surface roughness).

It can be seen from the given dependences that reflection from a pure tantalum film is 2–3 orders of magnitude higher than reflection from films consisting of tantalum/boron and tantalum/nitrogen compounds. It is also known [5] that pure Ta produced by magnetron sputtering is a polycrystalline film with relatively large crystallite sizes. This leads to the growth of roughness and internal stresses. Addition of boron provides an amorphous structure, whilst addition of nitrogen reduces internal stresses in the structure.

Since TaN and TaBN [9] are composite materials, modification of the ratio of elements may have a qualitative effect on the properties of both the absorber layer and the mask as a whole. This is a very significant factor for manufacturing lithographic masks. Therefore, in-process measurements are required and physical and optical properties of absorber materials shall be recovered in practice.

There are two most widely used techniques for experimental measurement of optical constants of materials. The first technique employs the measurement of thin film transmission coefficient [10–12]. For this, free-hanging thin film of the test material is formed. Generally, the film is deposited by magnetron sputtering onto a substrate with a sacrificial layer. Then the structure on the substrate is placed into liquid selective etch. The sacrificial layer is dissolved, the test film is recovered onto a supporting frame. Then, it is placed into a reflectometer. Radiation within a desired range is passed through the film. Radiation intensity before and after the film is measured to determined the absorption coefficient.

When using the Kramers–Kronig relation, the complex refractive index may be determined from the radiation absorption measurement. Since the EUV penetration depth is small (approximately 30 nm for Ta within 10–16 nm), ultrathin films are required for this type of measurements. For materials having relatively low absorption within the given range, films may reach thicknesses in the order of 100 nm. They may be easily produced and operated. But for tantalum-containing films, thickness shall not exceed

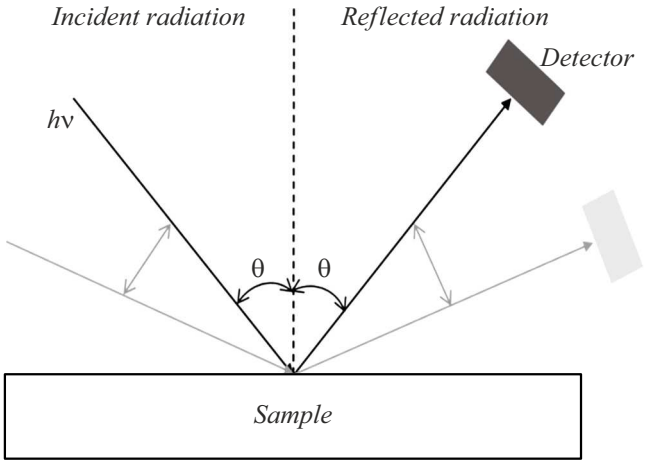

Figure 4. Schematic diagram of the experiment.

several tens of nanometers (20−30 nm). Formation of such thin films is a serious formidable technological challenge.

Another considerable problem for measurements in transmission mode is in that the optical properties of free-hanging thin films are not always identical to thin layers in stratified systems on substrates. This may be affected both by the presence of two interfaces with air for a free-hanging film and by consequences of the manufacturing process (for example, chemical contamination during wet etching). Therefore measurements on samples having a structure of a real optical component such as thin films on a substrate are much more promising.

The second approach to measuring optical properties of films is associated with reflectometry. The test film is studied directly on he substrate. And it is best to have the film in the same configuration as that used in practice. This is an ideal way to study, for example, a fully ready mask-blank, i.e. actually to qualify it before a pattern for lithography is made.

In this case, the reflection coefficient of radiation reflected from the given film is measured as function of the wavelength and angle of incidence [13,14]. Schematic diagram of the experiment is shown in Figure 4.

Reflection coefficient measurements with a variable wavelength and angle of incidence may be used to solve an inverse problem and recover structural parameters. There are more than one inverse problem solving method. A method used in this work is described in detail below.

Such experiments (measurement of thin-film system reflection coefficients) are usually carried out on a synchrotron radiation source. For example, such experiments were conducted at the Physikalisch-Technische Bundesanstalt (PTB) laboratory in a soft X-ray beamline of the Berliner Elektronenspeicherring-Gesellschaft für Synchrotronstrahlung (BESSY II) electron storage ring [15,16]. Employment of a synchrotron for measurements is obviously complicated in many cases. This may be due to a high workload and remote location of the existing synchrotron stations. Therefore an opportunity to perform measurements in laboratory conditions would have a favorable effect on work efficiency and research efforts in this field.

This study describes numerical opportunity analysis of whether laboratory reflectometry methods may be used for measuring optical constants of materials in EUV range.

1. Numerical experiment technique

The principal idea and novelty of the approach proposed by the authors are as follows.

First. It is a priori assumed that atomic scattering factors of atoms included in the test object are well known and tabulated, and are not used as a parameter for our fitting. Fitting parameters are fractions of these atoms in the test sample, densities and interlayer transition regions in films.

Second. Fitting is performed not separately for each curve, but rather simultaneously for a set of angular dependences of reflection coefficients at various wavelengths. Whilst the wavelength range shall be taken as wide as possible, preferably on both sides of the absorption jumps of materials included in the test structure. Such approach dramatically increases the recovery accuracy of densities and fractions of each material in the structure.

This study analyzed the simulated reflection curves obtained for the EUV and 0.154 nm hard X-ray radiation region. This wavelength (Cu Kαradiation line) is typical for widely used laboratory diffractometers. This is why it has been chosen.

The value of measurements at 0.154 nm is attributable to high sensitivity of hard X-ray radiation to film thicknesses and interfaces, and to determination of the system's mean refractive index. This radiation usually has high penetrating power (large extinction depth) and, thus, can characterize a thin-film structure with relatively extended depth.

Authors of most studies are guided by the critical angle when determining the structure's mean refractive index. However, the oxidized top layer has a large effect on the form of reflection curve in the full external reflection region both in hard and soft X-ray ranges, because a reflected wave at such sliding angles is formed primarily in the near-surface layer. For measurements at 0.154 nm, a lot of interference peaks are observed. These peaks are defined not only by a near-surface region, but also by the total structural depth. Angular positions of interference peaks are defined both by film thickness and refractive index (and its variation) of the films, i.e. by the refractive index throughout the structural depth (or radiation penetration depth). As the radiation sliding angle increases (actually as the interference peak number increases), the effect of the oxidized near-surface layer gets weaker, its contribution to the general reflected signal decreases, and peak positions are increasingly more accurately defined only by refraction in the structural films, i.e. by the optical properties of materials included in the structure itself.

The following laboratory instruments were described in this work:

— Philips X'Pert PRO ($\lambda = 0.154$ nm) diffractometer,

— reflectometer with Czerny –Turner monochromator.

Philips X'Pert PRO had a configuration with Ge (220) four-crystal monochromator. X-ray tube specifications are: $U_a = 30$ kV, $I_e = 20$ mA. Angular radiation divergence in the dispersion plane of test samples is 12 arc sec, sizes of monochromator outlet and detector inlet slits are set to $100-300\,\mu$m, slit heights are set to 10 mm. Angle scanning pitch is 0.002°. Dynamic range of probe beam intensity is 10^7. Mirror reflections are measured according to the $\theta-2\theta$ scheme, i.e. when the X-ray tube (radiation source) is fixed, rotation of the sample at θ is corresponded by the detector rotation at a doubled angle. For more details of diffractometer measurement conditions, see [17].

Soft X-ray and EUV reflective properties of thin-film coatings on substrates were measured at the Institute for Physics of Microstructures, Russian Academy of Sciences, using a measurement bench consisting of a reflectometer with laser plasma source and Czerny–Turner monochromator with improved spectral resolution [18]. Reflectometer's operating wavelength range is 5–60 nm. However, such wide range may be covered by changing the laser plasma source target and diffraction grating, spectrally-selective component. Our numerical experiments simulated measurements in the 10–16 nm spectral region with a gold target of the laser plasma source. Diffraction grating with a groove density of 900 groove/mm was chosen. Spectral resolution for such grating is better than 0.015 nm.

For the purpose of this study, the inverse problem was solved in Multifitting [19,20]. The software is based on an extended multilayer structure. To recover the internal structure using the X-ray reflectometry data, interlayer regions (interfaces) are represented in the form of a linear combination of functions corresponding to physical processes flowing during interface formation: material interdiffusion, chemical interaction, geometrical roughness growth. Multifitting is also distinguished by its capability to restore each structure using an arbitrary number of reflectometry curves simultaneously.

The following sequence of thin films on a Si wafer was used as a model structure in this work (Figure 5).

TaBN composite forms the basis of the test film. It is implied here that the TaBN film was deposited onto a single crystal silicon wafer in the synthesis process. An assumption was made that oxide could be formed at the film and air interface. A 2 nm TaBO layer was simulated here as such oxide. Similarly, 2 nm Ta_5Si_3 is formed between the film and wafer. Pure TaBN film thickness is 58 nm. The total thin-film system thickness is 62 nm. Densities for ρ-layer materials were taken from [5]. Roughnesses S were chosen randomly, but correspond by the order of magnitude to typical roughnesses for thin films.

It should be emphasized again that feasibility of this model system is not discussed here. For numerical experiment, other parameters could have been also taken. The key question is whether it is possible to restore the proposed model structure using reflectometry data.

Parameters of the given model structure served as input data for Multifitting. Then, angular reflection curves were simulated in this software:

— a wavelength of 0.154 nm in the angle range $0-7^\circ$ (Philips X'Pert PRO);

— a number of wavelengths from 10–16 nm at 0.3 nm intervals (10, 10.3, 10.6 nm, etc.) within $0-90^\circ$ (reflectometer with the Czerny–Turner monochromator).

The wavelength range was chosen according to the source intensity maximum position in the reflectometer with the Czerny–Turner monochromator and to the focus of the method made on determining optical constants of materials at 13.5 nm. The interval was chosen due to a desired structure recovery accuracy; as the interval increases to 1 nm, decrease in the relative accuracy by an order of magnitude is observed

Then, series of numerical experiments for reflection coefficient simulation depending on the wavelength and angle of incidence were conducted — a primal problem of X-ray reflectometry.

Multifitting calculates data with high accuracy. However, real instruments have a finite sensitivity and measurement error. Measurement errors were considered in our numerical experiments as follows.

For the Philips X'Pert PRO, due to its high sensitivity, data with a signal level lower than 10^{-7} with respect to the absolute reflection coefficient were dropped. A random error at each measurement point was also considered because the number of photons striking the test sample was sufficiently large and a term depending on the reflection coefficient could be neglected. Thus, an expression for the random instrument error is derived:

$$X = X + X(-1 + 2\,\mathrm{rnd})\left(\frac{7}{100\,000}\right). \qquad (1)$$

Here, $X$is the reflection coefficient, rnd is the random number generator function in the range from 0 to 1.

Other setting were taken for measurements using the reflectometer with the Czerny–Turner monochromator. Instrument sensitivity was lower, therefore data for a reflection coefficient lower than 10^{-3} were dropped. Error associated with the signal considered the amount of photons reaching the sample. Reflection coefficient is defined as

$$R = \frac{N_R}{N_i}, \qquad (2)$$

where N_R and N_i are the amount of reflected and incident photons, respectively. Relative error of the refrection coefficient is

$$\varepsilon_R = \sqrt{\frac{\overline{N}_i^2}{\overline{N}_R^2}\left(\frac{\Delta N_R^2}{\overline{N}_i^2} + \frac{\overline{N}_R^2(\Delta N_R)^2}{\overline{N}_i^4}\right)} = \sqrt{\varepsilon_{N_i}^2 + \varepsilon_{N_R}^2}. \qquad (3)$$

Main results of the study

Description	Model values (Figure 5)	Variation region	Replication 1	Replication 2	Replication 3	Replication 4
Amount of Ta atoms in oxide	1	1–3	2.952	1.498	2.995	1.858
Amount of O atoms in oxide	1	1–3	2.954	1.497	2.995	1.851
Amount of B atoms in oxide	1	1–3	2.952	1.501	2.990	1.859
Oxide-air interface roughness, Å	10	8–12	9.996	9.999	10.005	9.993
Oxide density, g/cm^3	9.2	8–11	9.184	9.192	9.215	9.187
Oxide layer thickness, angstrom	20	10–30	19.9694	19.9827	20.0249	19.9812
Amount of Ta atoms in film	1	1–3	2.248	1.976	1.352	2.058
Amount of B atoms in film	1	1–3	2.237	1.977	1.355	2.052
Amount of N atoms in film	1	1–3	2.252	1.975	1.351	2.062
Oxide-air interface roughness, angstrom	12	10–14	12.024	12.015	11.984	12.007
Film density TaBN, g/cm^3	13.5	12–15	13.501	13.501	13.5	13.499
Film thickness, Å	580	400–700	580.0455	580.031	579.964	580.019
Amount of Ta atoms in silicide	5	2–8	8	3.636	3.379	3.516
Amount of Si atoms in silicide	3	2–6	4.825	2.189	2.001	2.053
silicide-film interface roughness, Å	3	1–5	2.999	2.999	3.001	3.001
Silicide density, g/cm^3	11.282	10–13	11.281	11.282	11.286	11.289
silicide layer thickness, Å	20	10–30	19.9991	19.9976	20.0023	20.0048
silicide-substrate interface roughness, Å	3	1–5	3	3	3	2.999

According to the Poisson statistic, it is equal to

$$\sqrt{\varepsilon_{N_i}^2 + \varepsilon_{N_r}^2} = \sqrt{\frac{1}{N_i} + \frac{1}{N_R}}. \quad (4)$$

From the previous equation, relation for relative measurement error of reflection coefficient ε_R can be derived The amount of Ni photons was taken equal to $2 \cdot 10^6$ photons, this affected the signal as follows:

$$\varepsilon_R(N_i) = \sqrt{\frac{1}{N_i} + \frac{1}{RN_i}}\#. \quad (5)$$

Thus, the following expression for considering the error in an experiment is derived:

$$X = X + X(-1 + 2\,\mathrm{rnd})\varepsilon_R(N_i). \quad (6)$$

These parameters were added to the simulated curves of reflection from the structure shown in Figure 5.

The main objective of this work was to determine the reliability of recovered electron density distribution of a multicomponent thin film on substrate according to reflectometry data obtained using laboratory instruments with the defined accuracy on a laboratory X-ray source.

When solving the problem of structural parameter recovery, assumptions were made according to some a priori data. In particular, the presence of tantalum, boron and nitrogen, oxygen and silicon in the layers was supposed to be known. This assumption is believed to be reasonable because pure and well known materials are generally used in real synthesis. However, material ratios in the formed layers may differ from those planned for synthesis, and therefore are also a subject of research. Differences may

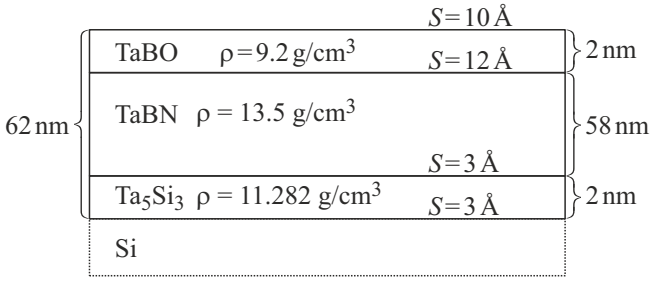

Figure 5. Model structure parameters

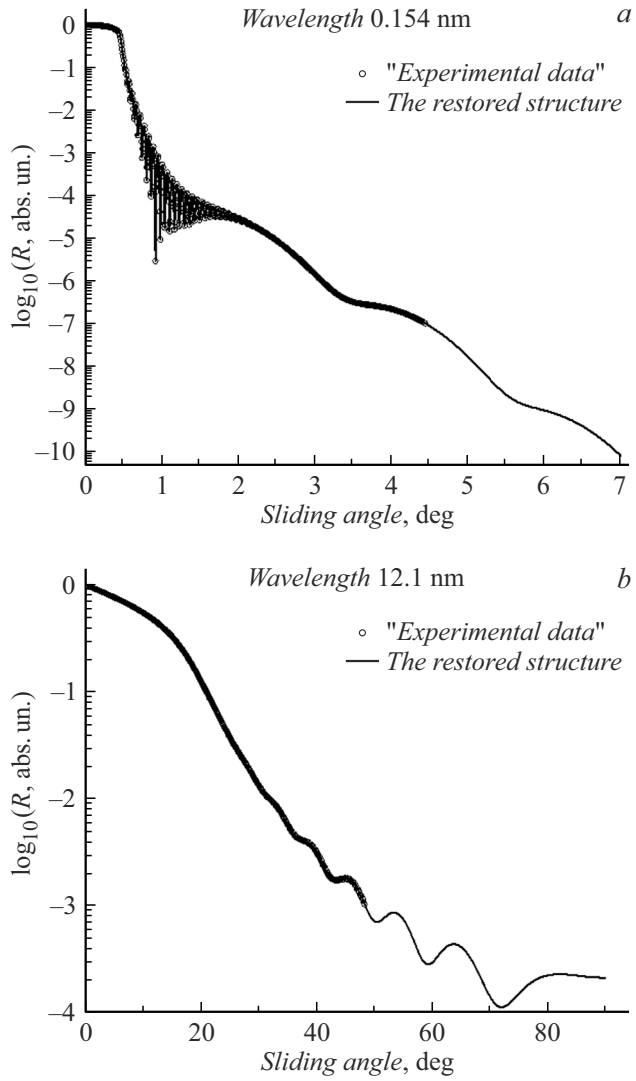

Figure 6. Comparison of „experimental“ reflection data at 0.154 (*a*) and 12.1 nm (*b*) with theoretical data from the restored structure.

result from the multicomponent film synthesis process. In particular, TaBN film is formed by magnetron sputtering of TaB target in argon and nitrogen mixture. While Ta and B atom ratios in the first approximation still can meet the magnetron target ratio (but this was not determined), then the amount of nitrogen embedded during growth is unknown.

For these ratios and other fitting parameters (roughnesses, layer thicknesses, densities), variation regions were defined. These regions are shown in the third column of the table. Actually, the parameter variation limits were chosen here at random. But this was not essential for the method of interest. In other particular experiments, limits may differ from the chosen ones. They also may rely on some a priori ideas of the subject of research.

After having selected the variation parameters, an inverse problem was solved and structure was restored in Multifitting taking into account the variation limits. To determine how much this solution was close to a true one, this operation was repeated 4 times.

2. Results

The main results of the study are listed in the table. The first column corresponds to the parameter of interest. The second column is a value of the parameter in accordance with the model (Figure 5). The third column is the parameter variation region in the numerical experiment. Fourth to seventh columns contain the values of parameters obtained in four replications within the numerical experiment.

Figure 6 shows the examples of simulated reflectometry data and fitting results for wavelengths of 0.154 nm and 12.1 nm.

Conclusion

The following conclusions can be drawn from the data provided. First, such structural parameters as densities, roughnesses and thicknesses can be recovered with high accuracy. Deviations of values obtained in all replications from the simulated values are much lower than 1%. Second, absolute amounts of atoms in layers fluctuate between variations within the defined determination region. However, element ratio in films is defined by high accuracy.

Thus, the numerical experiment shows that laboratory reflectometry is applicable to identification of parameters of thin films on substrates. Experimental validation of this conclusion will be the next step in our research.

Funding

Analysis of opportunities and determination of reflectometer accuracies, and experimental determination were supported by grant of the Russian Science Foundation 21-72-30029-P, development of the method and solution of the inverse problem were supported by grant of the Russian Science Foundation 21-72-20108-P.

Conflict of interest

The authors declare no conflict of interest.

References

[1] O. Wood, J. Arnold, T. Brunner, M. Burkhardt, J.H.-C. Chen, D. Civay, S.S.-C. Fan, E. Gallagher, S. Halle, M. He, C. Higgins, H. Kato, J. Kye, Ch.-S. Koay, G. Landie, P. Leung, G. McIntyre, S. Nagai, K. Petrillo, S. Raghunathan, R. Schlief, L. Sun, A. Wagner, T. Wallow, Yu. Yin, X. Zhu, M. Colburn, D. Corliss, C. Smolinski. Proceed. SPIE, **8322**, 832203 (2012). DOI: 10.1117/12.916292

[2] N.I. Chkhalo, N.N. Salashchenko. AIP Advances, **3** (8), 082130 (2013).

[3] T. Watanabe, T. Harada, S. Yamakawa. Proc. SPIE, **11908**, 1190807 (2021). DOI: 10.1117/12.2600896
[4] H. Levinson. *Principles of Lithography,* 4th ed. (SPIE, 2019), p. 524.
[5] Hoya Corporation, Morio Hosoya. *REFLECTIVE MASK BLANK AND METHOD OF MANUFACTURING A REFLECTIVE MASK* (Pattent US No.: 8,709,685 B2 29.04.2014)
[6] T. Liang, E. Ultanir, G. Zhang, S.-J. Park, E. Anderson, E. Gullikson, P. Naulleau, F. Salmassi, P. Mirkarimi, E. Spiller, Sh. Baker. J. Vacuum Sci. Technol. B, **25** (6), 2098 (2007). DOI: 10.1116/1.2779044
[7] S. Braun, H. Mai, M. Moss, R. Scholz, A. Leson. Jpn. J. Appl. Phys., **41** (6S), 4074 (2002).
[8] S.Yu. Zuev, R.S. Pleshkov, V.N. Polkovnikov, N.N. Salashchenko. M.V. Svechnikov, N.I. Chkhalo, F. Schäfers, M.G. Sertsu, A. Sokolov. ZhTF, **89** (11), 1779 (2019). DOI: 10.21883/JTF.2019.11.48344.130-19
[9] T. Shoki, M. Hosoya, T. Kinoshita, H. Kobayashi, Y. Usui, R. Ohkubo, Sh. Ishibashi, O. Nagarekawa. *Process development of 6-in EUV mask with TaBN absorber,* Proc. SPIE 4754, Photomask and Next-Generation Lithography Mask Technology IX, (1 August 2002). DOI: 10.1117/12.477007
[10] F. Delmotte, J. Meyer-Ilse, F. Salmassi, R. Soufli, C. Burcklen, J. Rebellato, A. Je'Rome, I. Vickridge, E. Briand, E. Gullikson. J. Appl. Phys., **124**, 035107 (2018).
[11] R. Soufli, F. Delmotte, J. Meyer-Ilse, F. Salmassi, N. Brejnholt, S. Massahi, D. Girou, F. Christensen, E.M. Gullikson. J. Appl. Phys., 125, 085106 (2019).
[12] M. Svechnikov, N. Chkhalo, A. Lopatin, R. Pleshkov, V. Polkovnikov, N. Salashchenko, F. Schäfers, M.G. Sertsu, A. Sokolov, N. Tsybin. J. Synchrotron Rad., **27**, 75 (2020). DOI: 10.1117/1.OE.60.4.044103
[13] R. Ciesielski, Q. Saadeh, V. Philipsen, K. Opsomer, J.-P. Soulié, M. Wu, P. Naujok, R.W.E. van de Kruijs, Ch. Detavernier, M. Kolbe, F. Scholze, V. Soltwisch. Appl. Optics, **61** (8), 2060 (2022). DOI: 10.1364/AO.447152
[14] V. Soltwisch, S. Glabisch, A. Andrle, V. Philipsen, Q. Saadeh, S. Schröder, L. Lohr, R. Ciesielski, S. Brose. *High-precision optical constant characterization of materials in the EUV spectral range: from large research facilities to laboratory-based instruments.* Proc. SPIE 12472, 37th European Mask and Lithography Conference, 124720Q (1 November 2022). DOI: 10.1117/12.2640176
[15] F. Scholze, J. Tümmler, G. Ulm. Metrologia, **40**, S224 (2003).
[16] F. Scholze, C. Laubis, C. Buchholz, A. Fischer, S. Ploeger, F. Scholz, H. Wagner, G. Ulm. Proc. SPIE, **5751**, 749 (2005).
[17] S.S. Andreev, A.D. Akhsakhalyan, M.A. Bibishkin, N.I. Chkhalo, S.V. Gaponov, S.A. Gusev, E.B. Kluenkov, K.A. Prokhorov, N.N. Salashchenko, F. Schäfers, S.Yu. Zuev. Centr. Europ. J. Phys., **1**, 191 (2003).
[18] S.A. Garakhin, N.I. Chkhalo, I.A. Kas'kov, A.Ya. Lopatin, I.V. Malyshev, A.N. Nechay, A.E. Pestov, V.N. Polkovnikov, N.N. Salashchenko, M.V. Svechnikov, N.N. Tsybin, I.G. Zabrodin, S.Yu. Zuev. Rev. Sci. Instrum., **91** (6), 063103 (2020). DOI: 10.1063/1.5144489
[19] M. Svechnikov. J. Appl. Crystallogr., **53** (1), 244 (2020). DOI: 10.1107/S160057671901584X
[20] M. Svechnikov. J. Appl. Cryst., **57**, 848 (2024). DOI: 10.1107/S1600576724002231

Translated by E.Ilinskaya